

Article

Half-Metallic Property Induced by Double Exchange Interaction in the Double Perovskite $\text{Bi}_2\text{BB}'\text{O}_6$ ($B, B' = 3d$ Transitional Metal) via First-Principles Calculations

Hong-Zong Lin ¹, Chia-Yang Hu ², Po-Han Lee ^{3,4,*}, Albert Zhong-Ze Yan ⁵, Wen-Fang Wu ⁶, Yang-Fang Chen ² and Yin-Kuo Wang ^{7,*}

¹ Institute Industrial Engineering of National Taiwan University, Taipei 10617, Taiwan; aj130820@gmail.com

² Department of Applied Physics, College of Science, National Taiwan University, Taipei 10617, Taiwan; younger978@gmail.com (C.-Y.H.); yfchen@phys.ntu.edu.tw (Y.-F.C.)

³ Department of Electro-Optical Engineering, National Taipei University of Technology, Taipei 10608, Taiwan

⁴ Affiliated Senior High School of National Taiwan Normal University, Taipei 10658, Taiwan

⁵ University of Southern California, Dornsife College of Letters, Arts, and Sciences, Los Angeles, CA 90089, USA; albertyanalbert@gmail.com

⁶ Department of Mechanical Engineering, National Taiwan University, Taipei 10617, Taiwan; wfwu@ntu.edu.tw

⁷ Center for General Education and Department of Physics, National Taiwan Normal University, Taipei 10610, Taiwan

* Correspondence: phlee@ntut.edu.tw (P.-H.L.); kant@ntnu.edu.tw (Y.-K.W.)

Received: 19 March 2019; Accepted: 3 June 2019; Published: 6 June 2019



Abstract: In this paper, we identify three possible candidate series of half-metals (HM) from Bi-based double perovskites $\text{Bi}_2\text{BB}'\text{O}_6$ ($\text{BB}' =$ transition metal ions) through calculations utilizing the density functional theory (DFT) and full-structural optimization, in which the generalized gradient approximation (GGA) and the strong correlation effect (GGA + U) are considered. After observing the candidate materials under four types of magnetic states, i.e., ferromagnetic (FM), ferrimagnetic (FiM), antiferromagnetic (AF), and nonmagnetic (NM), we found eight promising candidates for half-metallic materials. Under the GGA scheme, there are three ferromagnetic-half-metal (FM-HM) materials, $\text{Bi}_2\text{CrCoO}_6$, $\text{Bi}_2\text{CrNiO}_6$ and $\text{Bi}_2\text{FeNiO}_6$, and three FiM-HM materials, $\text{Bi}_2\text{FeZnO}_6$, $\text{Bi}_2\text{CrZnO}_6$ and $\text{Bi}_2\text{CoZnO}_6$. With implementation of the Coulomb interaction correction (GGA + U), we find two stable half-metallic materials: $\text{Bi}_2\text{CrNiO}_6$ and $\text{Bi}_2\text{CrZnO}_6$. We determine that the stability of some of these materials are tied to the double exchange interaction, an indirect interaction within the higher powers of localized spin interaction among transition metals via oxygen ions. Found in half-metallic materials, and especially those in the ferromagnetic (FM) state, the double exchange interaction is recognized in the FM-HM materials $\text{Bi}_2\text{CrCoO}_6$ and $\text{Bi}_2\text{FeNiO}_6$.

Keywords: double perovskite; first-principle calculations; half-metal; double exchange; ferrimagnetic state

1. Introduction

Valued for their application in spintronic devices, half-metallic (HM) materials are useful based on their three distinguishing features: 100% spin polarization at the Fermi level (E_F), quantization of magnetic moment, and zero spin susceptibility. Half-metals are characterized by an energy gap existing in one spin channel, showing insulating behavior, and no energy gap in the other spin channel, showing metallic behavior. This makes half-metallic materials particularly suitable for application in

technologies such as computer memory manipulation, magnetic recording, single-spin electron source measurement, and high-efficiency magnetic sensors [1,2]. Some previously discovered half-metal materials include the doped perovskite structure manganese oxide $\text{La}_{0.7}\text{Sr}_{0.3}\text{MnO}_3$ [1], spinel Fe_3O_4 [2], rutile CrO_2 [3], double perovskites $\text{Sr}_2\text{FeMoO}_6$ [4–9], La_2VTcO_6 and La_2VCuO_6 [10], doped perovskite structure manganese oxide $\text{La}_{0.5}\text{Ca}_{0.5}\text{MnO}_3$ [11], Mn-doping $\text{Mn}_x\text{Ga}_{1-x}\text{N}$ [12], spinel FeCr_2S_4 [13], and Mn-doping GaAs [14,15].

In the search for new half-metallic materials, the double perovskite structure is a suitable template due to its flexibility and ease of illustrating an abundance of material properties, such as band insulators, ferromagnets, and ferroelectrics [3,16–18]. Organic double perovskites have recently been utilized for their remarkable optoelectronic properties [19–25]. Traditional photoelectrochemical cells, usually equipped with organic sensitizers and inorganic semiconductors, carry certain limitations that often result in low absorption coefficients and narrow absorption bands in these solar cells. However, seminal work by Kojima et al. in 2009 proposed a new material design based on organic-inorganic lead halide perovskite compounds $\text{CH}_3\text{NH}_3\text{PbBr}_3$ and $\text{CH}_3\text{NH}_3\text{PbI}_3$ in which a $\text{CH}_3\text{NH}_3\text{PbI}_3$ -based cell is able to convert solar energy with an efficiency of 3.8% and a $\text{CH}_3\text{NH}_3\text{PbBr}_3$ -based cell is able to gain a high photovoltage of 0.96 V [19]. Since this milestone, related research has been experiencing exponential growth to the point that photovoltaic efficiency has been able to reach above 22% [20]. There are also other designs of solar cells, such as efficient solar cells using iodide management in formamidinium-lead-halide-based perovskite layers, with a power conversion efficiency of 22.1% in small cells [22]. Furthermore, metal-halide perovskite semiconductors related to solar energy conversion have also become a hot topic [23,24]. Some Pb-free, stable inorganic double halide perovskites have been looked into as well since Pb is a pollutant element in our environment [25].

However, our studies focus on inorganic double perovskites, such as the Sr-based double perovskites $\text{Sr}_2\text{BB}'\text{O}_6$, including $\text{Sr}_2\text{FeMoO}_6$ [4–9], $\text{Sr}_2\text{FeReO}_6$ [5,26], Sr_2FeWO_6 [6], $\text{Sr}_2\text{CrMoO}_6$ [7], $\text{Sr}_2\text{CrReO}_6$ [26,27], and Sr_2CrWO_6 [5,28], all of which are HM materials. We use an $\text{A}_2\text{BB}'\text{O}_6$ structure constructed by two different ternary perovskites, ABO_3 and $\text{AB}'\text{O}_3$, where the A-site elements are substituted with alkaline earth or rare-earth ions, such as Ca, Sr, Ba, and La, and the B-site elements are substituted with transition metal ions, utilized for their diverse electronic configurations in d-orbitals and juxtaposition due to the strong interaction. Dissimilarities in size and valence between the B and B' ions are vital in controlling the physical properties of these materials [29,30]. By exploring a multitude of compounds based on this structure, we can easily identify suitable HM candidates.

2. Materials and Methods

This paper mainly focuses on the search for HM materials from inorganic double perovskite compounds. Accordingly, we expand on previous outcomes and execute calculations in the area of Bi-based double perovskites $\text{Bi}_2\text{BB}'\text{O}_6$ ($B, B' = 3d$ transition metal) with consideration of 4 types of initial magnetic states, namely ferromagnetic (FM), ferrimagnetic (FiM), antiferromagnetic (AF), and nonmagnetic (NM), with a total of 45 (C_2^{10}) compounds of $\text{Bi}_2\text{BB}'\text{O}_6$ series in these studies. Additionally, we compare the AF calculations of these materials with their FM-based calculations. After the process of full structural optimization, we attempt to find out how many cases of stable HM materials are left and analyze the d-orbital distributions of the density of states (DOS) in these materials. We go a step further and determine the cases of HM materials in view of the strong correlation correction (GGA + U) as well.

We also investigate the effect of the double exchange (DE) interaction within these HM candidates. The first proposal of DE was presented by Zener [31], who considered the DE to involve simultaneous jumps between two electrons. A second description was proposed by Anderson and Hasegawa [32] who considered DE to be the transfer process in which a mobile electron is able to move one Mn ion to the other Mn ion by the so-called local exchange. Some theoretic and calculation works related to the DE effect are described in detail in previous studies [8,9,17,33–36].

2.1. Structural Optimization

To utilize and calculate an atomic model, it is often necessary to have structural optimization to ensure accuracy. In order for the ideal cubic structure (space group of $Fm\bar{3}m$, No. 225) to be assigned as the F(i)M or AF state, we have to organize the B and B' ions in the order of a NaCl configuration with a lattice constant of $2a$. According to this ordering, the $B(B')$ elements are equipped with transition metals with an O ion placed evenly between each pair. For an ideal cubic structure, the c/a ratio is set to $\sqrt{2}$. To understand the observed stable states in the condition of a supercell (2 formula units [f.u.]), we relax this cubic structure to a reduced symmetry through structural optimization calculations.

Next, we determine whether the structures are stable after full structural optimization, resulting in two structures being discussed. One of them is the tetragonal structure (space group of $I4/mmm$, No. 139) accompanied by two non-equivalent types of O atoms, in which two O_1 atoms are located on the z -axis and four O_2 atoms are located on the xy -plane, as shown in Figure 1. Accordingly, these are the cases of F(i)M state. The other one is the tetragonal structure (space group of $P4/mmm$, No. 123) with non-equivalent types of O atoms, in which the angle of $B-O_1-B'$ remains at 180° and the angle of $B-O_2-B'$ has been altered a little but is still close to 180° during structural optimization. This means the symmetry reduction is deemed rather minor and the c/a ratio is very close to the value of $\sqrt{2}$. This final structure is found in the AF state.

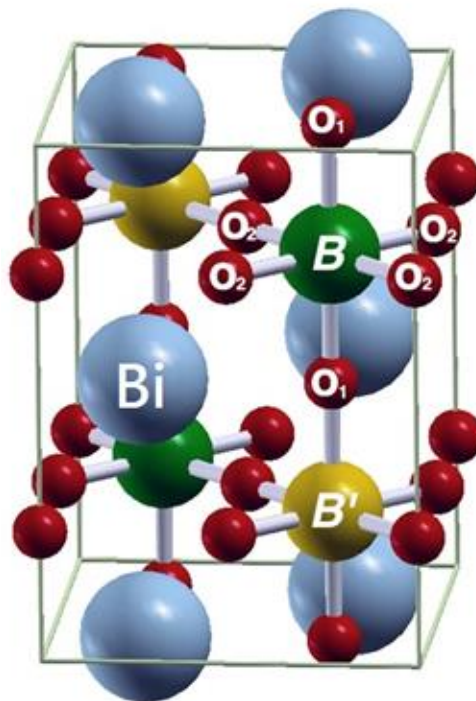


Figure 1. An ideal ordered double perovskites structure $Bi_2BB'O_6$. ($B, B' = 3d$ transition metal).

2.2. Calculation Method and Procedure

For the initial magnetic configuration of the B ion pairs and B' ion pairs, we assign the magnetic states for the initial stage based on the four states of FM, FiM, AF, and NM, as shown in Figure 2. The spin alignment of FM state is assigned as $(B, B, B', B') = (m, m, m', m')$, the spin alignment of FiM state is assigned as $(B, B, B', B') = (m, m, -m', -m')$, and AF as $(B, B, B', B') = (m, -m, m', -m')$. For NM, there is no spin assigned initially. All the cases begin with the ideal cubic structure belonging to the space group $Fm\bar{3}m$.

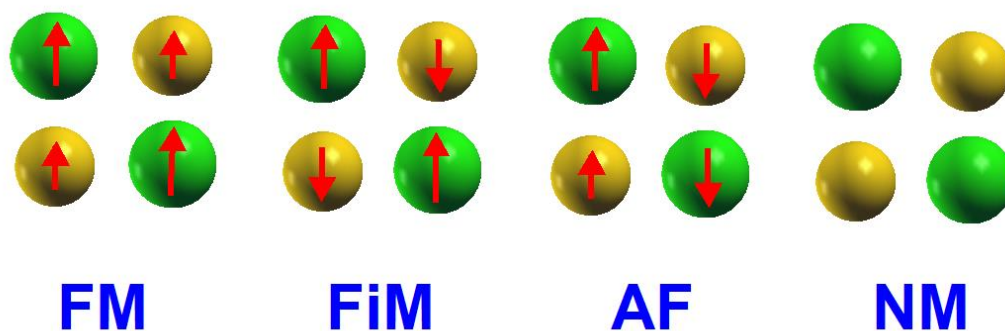


Figure 2. The schematic diagram of 4 magnetic states: FM, FiM, AF, and NM.

By going through the process of full structural optimization in the GGA scheme, some cases for FM and FiM states converge into the other state, while others remain in their initial states. Furthermore, we assign the magnetic case as half-metallic anti-ferromagnetic (HM-AF) if the summation of the total magnetic moment with an initial FiM state becomes zero [10] and the induced symmetry of the spin-up and spin-down orbitals exists in the total density of state (DOS). The cases related to the calculations of spin polarization have always been more stable than those of the NM state.

The calculations are based on Density Functional Theory (DFT) [37] and the full-potential projector augmented wave method [38], which is implemented in the Vienna Ab initio Simulation Package (VASP) code [39–41]. In searching for stable structures and stable ionic positions, we choose the full structural optimization process to relax both lattice constants and atomic positions, while applying the conjugate-gradient method to relax the ionic positions. The related parameters are set as follows: the energy convergence criteria for self-consistent calculations is set as 10^{-6} eV, $8 \times 8 \times 6$ k -point grids are used for the Brillouin zone, the cut-off energy of the plane wave basis is set as 450 eV, the Wigner–Seitz radius of the Sr atom set as 2.5 atomic units (a.u.), 1.4 a.u. for O atom, and 2.1 a.u. as $B(B')$ ion. For the final and equilibrium structures, the forces and stresses acting on all the atoms were less than 0.03 eV/Å and 0.9 kBar, respectively.

After the structural optimization, the F(i)M generally reduces to a tetragonal structure (space group of $I4/mmm$, No. 139), while the AF state will be in a different tetragonal structure (space group of $P4/mmm$, No. 123). The NM state is always unstable in consideration of the energy difference between the other states. Hence, we will exclude the discussion of NM cases in the following sections. Another condition that will be taken into account is the electron correlation correction (GGA + U), which will be applied for all the cases. We choose the effective parameter U_{eff} , $U - J$, where U is defined as the Coulomb potential and J as the exchange parameters.

In this paper, the parameter U_{eff} is denoted as U for simplicity in the functions of the d orbital. Dealing with the transition metals, the nearly maximum values are selected from a reasonable range of U [42]. In this study, consequently, U values were assigned as 2.0, 3.0, 4.0, 5.0, 6.0, 6.0, 7.0, and 7.0 for Sc, Cr, Mn, Fe, Co, Ni, Cu, and Zn, respectively. Near maximum is chosen because when considering two cases of initial $U = 0$ and less than $0.5 \times U$, the calculation results with less than $0.5 \times U$ are almost the same in comparison with the case of $U = 0$. Therefore, selecting the nearly maximum values of U is needed when trying to disclose the results from strong Coulomb interaction in these compounds.

3. Results and Discussion

After the process of full structural optimization, 8 of the 45 compounds in the $\text{Bi}_2\text{BB}'\text{O}_6$ series were categorized as HM materials. These include 6 compounds in the GGA scheme, namely $\text{Bi}_2\text{CrCoO}_6$, $\text{Bi}_2\text{CrNiO}_6$, and $\text{Bi}_2\text{FeNiO}_6$ as FM-HM materials, and $\text{Bi}_2\text{FeZnO}_6$, $\text{Bi}_2\text{CrZnO}_6$ and $\text{Bi}_2\text{CoZnO}_6$ as FiM-HM materials. With the scheme of (GGA + U), 2 stable half-metallic (HM) materials $\text{Bi}_2\text{CrNiO}_6$ (FM-HM) and $\text{Bi}_2\text{CrZnO}_6$ (FiM-HM) are found. Figures 3–8 describe the DOS and the partial DOS (PDOS) for these 6 FM/FiM-HM stable materials in the order of $\text{Bi}_2\text{CrCoO}_6$, $\text{Bi}_2\text{CrNiO}_6$, $\text{Bi}_2\text{FeNiO}_6$, $\text{Bi}_2\text{FeZnO}_6$, $\text{Bi}_2\text{CrZnO}_6$, and $\text{Bi}_2\text{CoZnO}_6$, respectively. Figures 9 and 10 illustrate the 2 AF-based

compounds, $\text{Bi}_2\text{CrCoO}_6$ and $\text{Bi}_2\text{FeNiO}_6$. For a clearer illustration of each $\text{Bi}_2\text{BB}'\text{O}_6$, every sub-Figure a represents the total DOS and sub-Figure b,c demonstrate the PDOS for B and B' atoms with the GGA scheme. Sub-Figure d-f represents the total DOS with the GGA + U scheme, and the PDOS for B and B' with the GGA + U scheme, respectively. To carefully monitor the strong-correlation correction (GGA + U) for transition metals, the U values are noted as ($U_B, U_{B'}$). After optimization, FM and FiM states converge, with structural parameters of their tetragonal structure ($I4/mmm$, No. 139) illustrated in Table 1. AF retains its state with the tetragonal structure ($P4/mmm$, No. 123). After fully optimizing $\text{Bi}_2\text{BB}'\text{O}_6$, two types of oxygen are labeled as O_1 and O_2 , of which the final stable positions of O_{1z} , O_{2x} and O_{2y} are listed in Table 1. The volume variations are slight for all the compounds, except for $\text{Bi}_2\text{CrZnO}_6$, which has the largest volume of $118.095 \text{ \AA}^3/\text{f.u.}$ In addition, the calculated physical properties and energy differences are listed in Table 2, where we are able to find energy differences, ΔE , between the FM and AF states. Table 3 indicates all the energy states for various final magnetic states in detail. The energy levels for the final NM states are all larger than those of AF and FM(FiM) by roughly 1000 meV or above, implying that the NM cases are unstable. This is why we have excluded the list of NM energy states here.

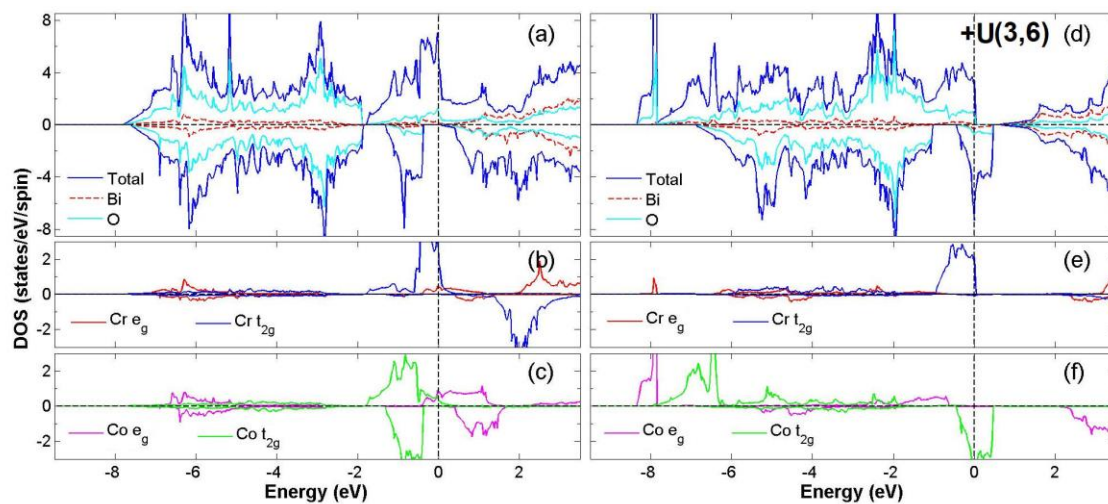


Figure 3. Calculated FM- $\text{Bi}_2\text{CrCoO}_6$ total Density of State (DOS) (a) and partial DOS of e_g and t_{2g} spin orbitals for Cr (b) and Co (c) under GGA and total DOS (d) partial DOS of e_g and t_{2g} spin orbitals for Cr (e) and Co(f) under GGA + U (Cr = 3, Co = 6) schemes.

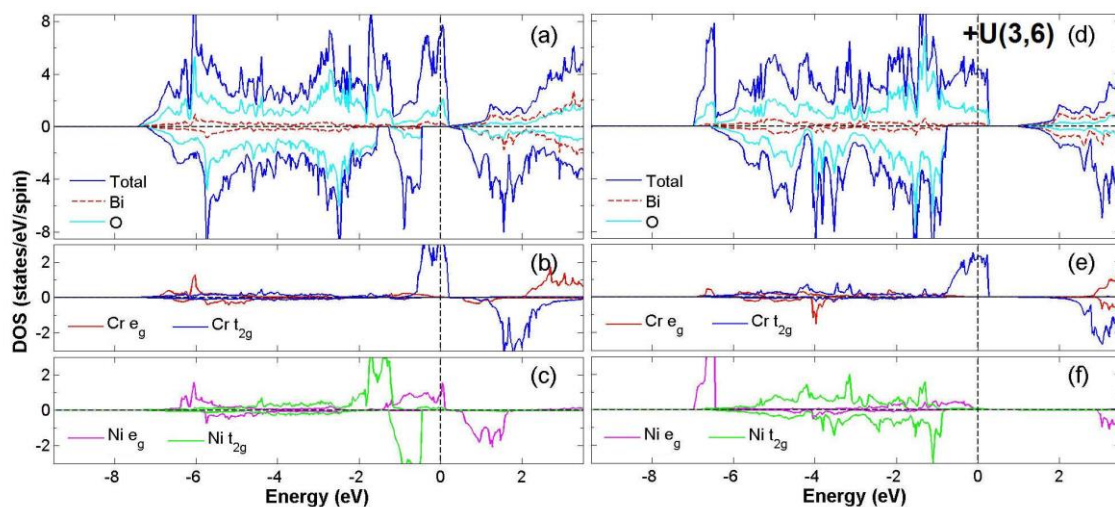


Figure 4. Calculated FM- $\text{Bi}_2\text{CrNiO}_6$ total DOS (a) and partial DOS of e_g and t_{2g} spin orbitals for Cr (b) and Ni (c) under GGA and total DOS (d) partial DOS of e_g and t_{2g} spin orbitals for Cr (e) and Ni (f) under GGA + U (Cr = 3, Ni = 6) schemes.

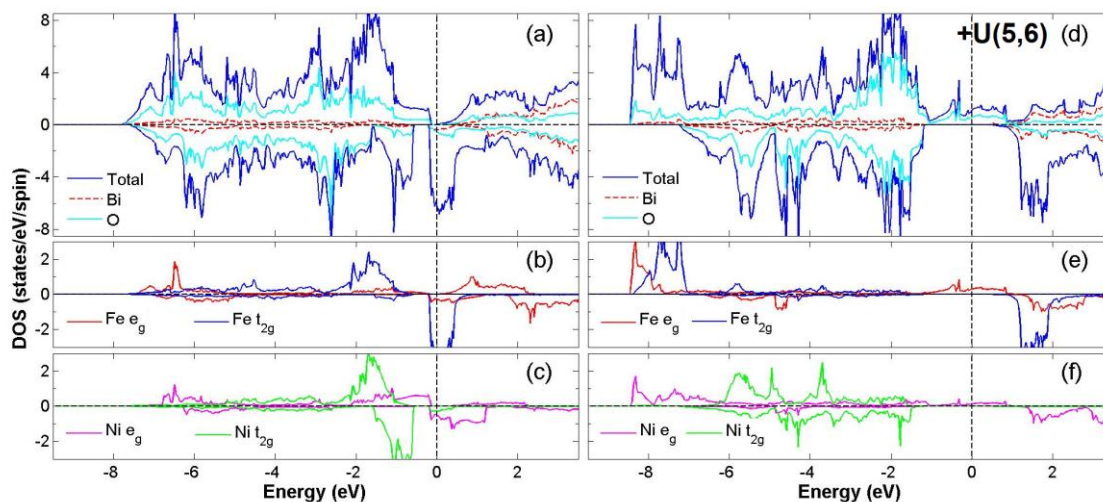


Figure 5. Calculated FM-Bi₂FeNiO₆ total DOS (a) and partial DOS of e_g and t_{2g} spin orbitals for Fe (b) and Ni (c) under GGA and total DOS (d); partial DOS of e_g and t_{2g} spin orbitals for Fe (e) and Ni (f) under GGA + U (Fe = 5, Ni = 6) schemes.

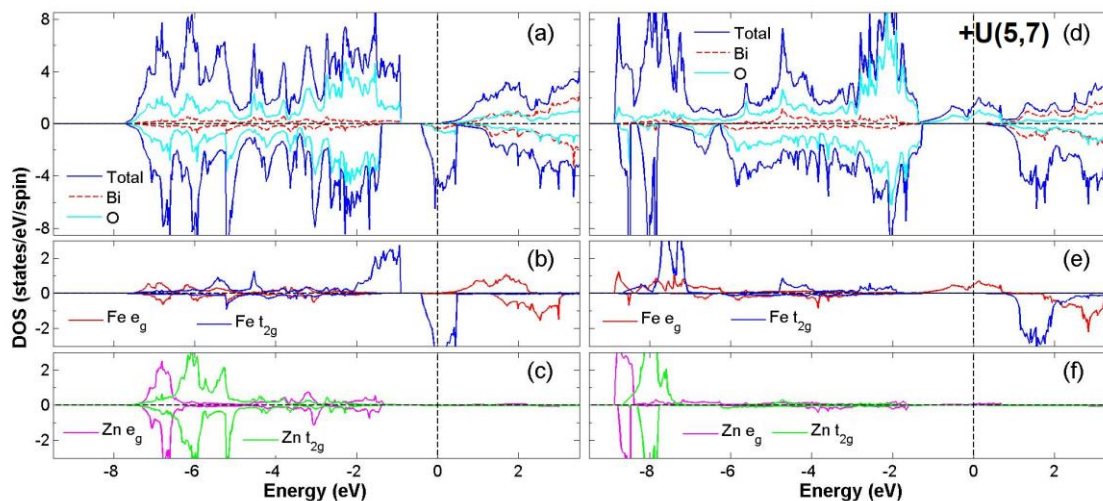


Figure 6. Calculated FiM-Bi₂FeZnO₆ total DOS (a) and partial DOS of e_g and t_{2g} spin orbitals for Fe (b) and Zn (c) under GGA and FM-Bi₂FeZnO₆ total DOS (d); partial DOS of e_g and t_{2g} spin orbitals for Fe (e) and Zn (f) under GGA + U (Fe = 5, Zn = 7) schemes.

Table 1. The final stable structure of tetragonal (I4/mmm, No. 139) and related parameters of the compounds which are fully optimized, where a , c are lattice constants, V_0 represents the compound volume per f.u. and Bi coordinates $(x, y, z) = (0, 0.5, 0.75)$, $B(x, y, z) = (0, 0, 0)$, $B'(x, y, z) = (0, 0, 0.5)$, $O_1(x, y, z) = (0, 0, O_{1z})$ and $O_2(x, y, z) = (O_{2x}, O_{2y}, 0.5)$ as illustrated in Figure 1.

$\text{Bi}_2\text{BB}'\text{O}_6$	a	c/a	V_0 ($\text{\AA}^3/\text{f.u.}$)	O_{1z}	O_{2x}	O_{2y}
CrCo	5.419	1.413	112.461	0.2528	0.2471	0.2471
CrNi	5.453	1.415	114.724	0.2473	0.2526	0.2526
FeNi	5.421	1.413	112.606	0.2453	0.2546	0.2546
FeZn	5.464	1.414	115.332	0.2399	0.2600	0.2600
CrZn	5.505	1.416	118.095	0.2414	0.2587	0.2587
CoZn	5.450	1.415	114.467	0.2400	0.2600	0.2600

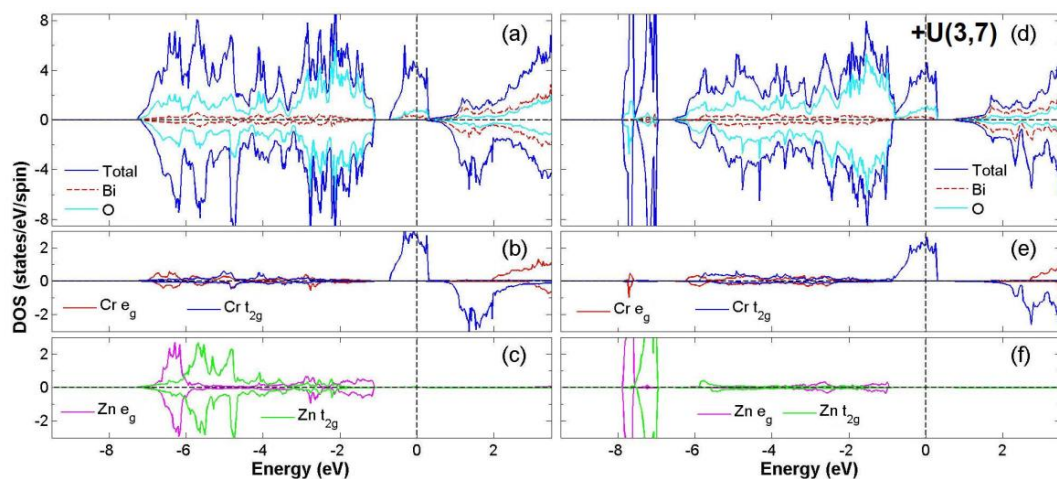


Figure 7. Calculated $\text{FiM-Bi}_2\text{CrZnO}_6$ total DOS (a) and partial DOS of e_g and t_{2g} spin orbitals for Cr (b) and Zn (c) under GGA and total DOS (d) partial DOS of e_g and t_{2g} spin orbitals for Cr (e) and Zn (f) under GGA + U (Cr = 3, Zn = 7) schemes.

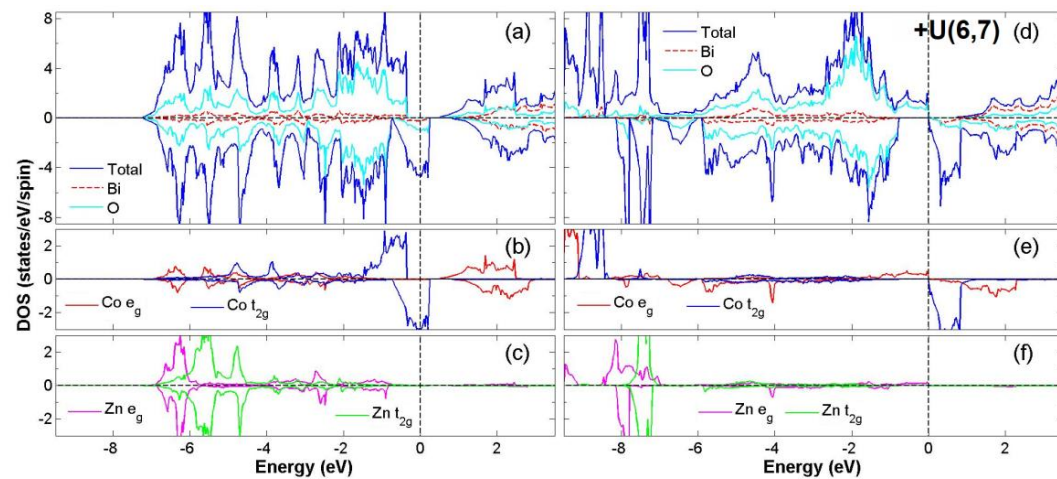


Figure 8. Calculated $\text{FiM-Bi}_2\text{CoZnO}_6$ total DOS (a) and partial DOS of e_g and t_{2g} spin orbitals for Co (b) and Zn (c) under GGA and $\text{FM-Bi}_2\text{CoZnO}_6$ total DOS (d) partial DOS of e_g and t_{2g} spin orbitals for Co (e) and Zn (f) under GGA + U (Co = 6, Zn = 7) schemes.

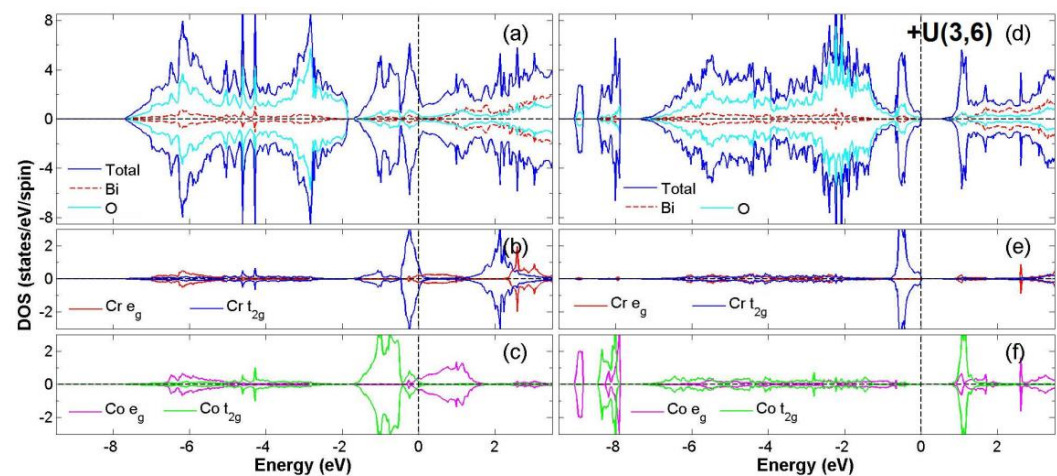


Figure 9. Calculated $\text{AF-Bi}_2\text{CrCoO}_6$ total DOS (a) and partial DOS of e_g and t_{2g} spin orbitals for Cr (b) and Co (c) under GGA and total DOS (d) partial DOS of e_g and t_{2g} spin orbitals for Cr (e) and Co (f) under GGA + U (Cr = 3, Co = 6) schemes.

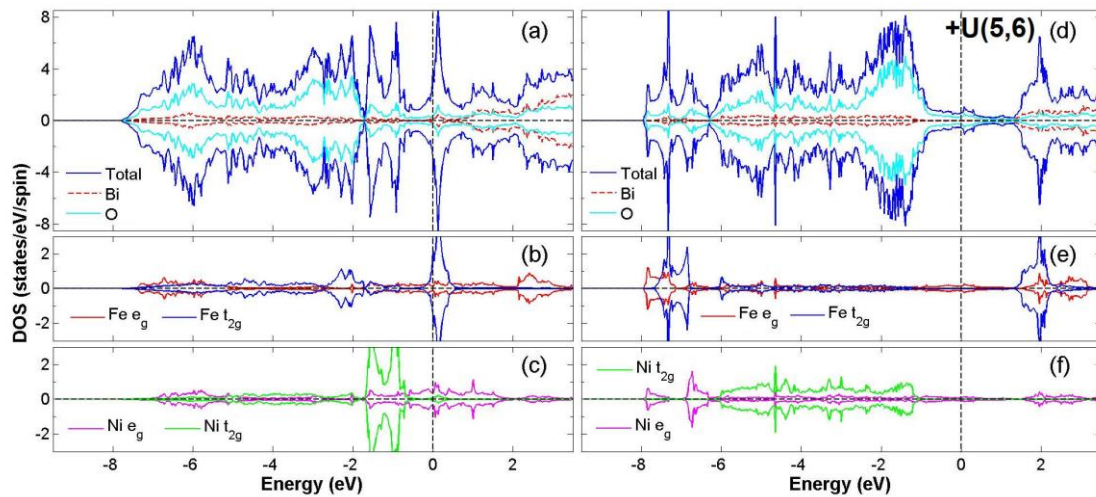


Figure 10. Calculated AF-Bi₂FeNiO₆ total DOS (a) and partial DOS of e_g and t_{2g} spin orbitals for Fe (b) and Ni (c) under GGA and total DOS (d) partial DOS of e_g and t_{2g} spin orbitals for Fe (e) and Ni (f) under GGA + U (Fe = 5, Ni = 6) schemes.

Table 2. Physical properties of the selected FM(FiM)-HM and AF family of Bi₂BB'O₆ (B , B' = 3d transition metal) with the full structural optimization calculation of GGA and GGA + U . In the table below, $U_{B(B')}$ are the effective parameters used in GGA + U calculations for $B(B')$. The spin magnetic moments for B , B' , and the total moment are listed in the table as m_B , $m_{B'}$, and m_{tot} respectively. Electrons in the spin up and spin down orbitals for $B(B')$ elements are listed as well.

Materials Bi ₂ BB'O ₆	$(U_B, U_{B'})$	Spin Magnetic Moment (μ_B /f.u.)			d Orbital Electrons \uparrow/\downarrow		Band Gap (eV)	ΔE (meV/f.u.) FM(FiM)
		m_B	$m_{B'}$	m_{tot}	B	B'		
CrCo	(0, 0)	2.573	0.162	3.000	3.465/0.927	3.749/3.575	0.00/0.40	-25
	(3, 6)	2.852	3.071	6.792	3.574/0.804	5.108/2.044	0.00/0.00	903
CrNi	(0, 0)	2.304	1.267	4.000	3.304/1.076	4.767/3.496	0.00/0.65	-97
	(3, 6)	2.303	1.703	4.000	3.272/1.036	5.019/3.320	0.00/1.73	-112
FeNi	(0, 0)	2.146	1.224	4.000	4.143/2.054	4.749/3.528	0.15/0.00	-43
	(5, 6)	3.887	1.644	6.000	4.919/1.094	4.939/3.341	0.00/1.68	34
FeZn	(0, 0)	1.694	-0.022	2.000	3.950/2.269	4.968/4.984	0.97/0.00	-58
	(5, 7)	3.66	0.015	4.000	4.848/1.223	5.022/5.051	0.00/1.52	1125
CrZn	(0, 0)	1.866	-0.013	2.000	3.111/1.274	4.981/4.988	0.00/1.30	-60
	(3, 7)	2.073	-0.008	2.000	3.202/1.165	5.050/5.054	0.00/1.57	-73
CoZn	(0, 0)	0.758	-0.013	1.000	3.995/3.242	4.966/4.976	0.85/0.00	-51
	(6, 7)	3.463	0.105	5.000	5.229/1.782	5.080/5.025	0.65/0.75	99
CrCo(AF)	(0, 0)	2.579	0.057	0.000	3.467/0.925	3.692/3.631	0.00/0.00	-
	(3, 6)	2.799	3.194	0.000	3.561/0.816	5.129/1.952	0.53/0.53	-
FeNi(AF)	(0, 0)	2.805	0.836	0.000	4.439/1.675	4.567/3.735	0.00/0.00	-
	(5, 6)	3.847	1.517	0.000	4.894/1.089	4.912/3.410	0.00/0.0	-

Table 3. The energy of the final states for $\text{Bi}_2\text{BB}'\text{O}_6$ ($B, B' = 3d$ transition metal) with the full structural optimization calculation of GGA and GGA + U . In the table below, $U_{B(B')}$ are the effective parameters used in GGA + U calculations for $B(B')$.

Materials $\text{Bi}_2\text{BB}'\text{O}_6$	$(U_B, U_{B'})$	Final State	E(eV/f.u.)	Materials $\text{Bi}_2\text{BB}'\text{O}_6$	$(U_B, U_{B'})$	Final State	E(eV/f.u.) (eV)
CrCo	(0, 0)	AF	−65.880	FeZn	(0, 0)	AF	−57.804
	(3, 6)	AF	−61.827	−	(5, 7)	AF	−56.040
	(0, 0)	FM	−65.905	−	(0, 0)	FiM	−57.862
CrNi	(3, 6)	FM	−60.924	−	(5, 7)	FM	−54.915
	(0, 0)	AF	−63.883	CrZn	(0, 0)	AF	−60.725
	(3, 6)	AF	−60.877	−	(3, 7)	AF	−58.949
	(0, 0)	FM	−63.980	−	(0, 0)	FiM	−60.785
FeNi	(3, 6)	FM	−60.989	−	(3, 7)	FiM	−59.022
	(0, 0)	AF	−61.036	CoZn	(0, 0)	AF	−55.693
	(5, 6)	AF	−57.053	−	(6, 7)	AF	−51.111
	(0, 0)	FM	−61.079	−	(0, 0)	FiM	−55.744
	(5, 6)	FM	−57.019	−	(6, 7)	FM	−51.012

3.1. FM-HM Compounds: $\text{Bi}_2\text{CrCoO}_6$, $\text{Bi}_2\text{CrNiO}_6$, and $\text{Bi}_2\text{FeNiO}_6$

Here, $\text{Bi}_2\text{CrCoO}_6$, $\text{Bi}_2\text{CrNiO}_6$, and $\text{Bi}_2\text{FeNiO}_6$ lean towards the FM state after structural optimization, of which the calculated total energy differences ($\Delta E = \text{FM} - \text{AF}$) are -25 , -97 , and -43 meV/f.u., respectively. These 3 cases are all stable FM-HM compounds in the GGA scheme. However, with the GGA + U scheme, the ΔE are 903, -112 , and 34 meV/f.u., respectively. Only $\text{Bi}_2\text{CrNiO}_6$ remains a stable FM-HM compound for both GGA and GGA + U schemes. The data are listed in Tables 2 and 3.

The band gaps occurs in the spin-down channel for the compounds $\text{Bi}_2\text{CrCoO}_6$ and $\text{Bi}_2\text{CrNiO}_6$, as shown in Figures 3a and 4a, while the band gap exists in the spin-up channel for $\text{Bi}_2\text{FeNiO}_6$ as shown in Figure 5a. Monitoring the location of the band gap near Fermi energy provides the most direct evidence for HM material. The second indicator for HM material is related to the integer value of total magnetic moments (m_{tot}), where $m_{\text{tot}} = 3.0 \mu_B/\text{f.u.}$ is noted for $\text{Bi}_2\text{CrCoO}_6$ (GGA), $4.0 \mu_B/\text{f.u.}$ for $\text{Bi}_2\text{CrNiO}_6$ (GGA and GGA + U), and $\text{Bi}_2\text{FeNiO}_6$ (GGA). However, there were two cases that lost the possibility of being HM material when the GGA + U scheme was considered. The first one was because the total magnetic moment of $\text{Bi}_2\text{CrCoO}_6$ changed from 3.0 to $6.792 \mu_B/\text{f.u.}$; the second case was when $\text{Bi}_2\text{FeNiO}_6$ lost its magnetic stability for FM when considering the energy of its AF state.

In these compounds, the p orbitals of Oxygen have two kinds of energy distributions for DOS. For example, in $\text{Bi}_2\text{CrCoO}_6$, the hybridization between Cr t_{2g} , O $2p$, and Co t_{2g} orbitals occurs mainly in the two energy ranges -7.5 eV to -2.5 eV and -2.0 eV to 0.5 eV, as illustrated in Figure 3a. The localized spin-to-spin interaction of double exchange was inferred from the interaction of $\text{Cr}t_{2g}\text{-O}2p\text{-Co}t_{2g}$. Such DE effect enhances the HM property of $\text{Bi}_2\text{CrCoO}_6$. Likewise, in $\text{Bi}_2\text{CrCoO}_6$, a band gap exists at the spin-down channel with the GGA scheme, but the gap disappears and its FM state becomes unstable once GGA + U is applied, thus losing its half-metal properties.

In the GGA scheme, the weak magnetic moment $0.162 \mu_B$ for Co is caused by the asymmetrical distribution of the Co e_g near the Fermi level as shown in Figure 3b,c, while in the GGA + U scheme, the stronger and non-integer magnetic moment of $3.071 \mu_B$ for Co is induced again from the variation of the t_{2g} orbital of Co. According to the energy listed in Table 2, there is a huge variation for $\text{Bi}_2\text{CrCoO}_6$ from GGA to GGA+ U scheme, -25 to 903 meV. For such a result, we have to take a deeper look into the PDOS of the Cr and Co atoms. When applying the GGA + U scheme for $\text{Bi}_2\text{CrCoO}_6$, the PDOS of Cr e_g near Fermi level is pushed to a higher energy level, while the Cr t_{2g} only changes a little. Furthermore, the PDOS of Co t_{2g} (spin-up) shifts back to a lower energy level, while the PDOS of Co t_{2g} (spin-down) is pushed to a higher energy level, crossing the Fermi energy and breaking the gap. There is a huge variation within the PDOS of Co e_g . All of these variations of PDOS result in the total energy value

changing from negative to positive. Consequently, AF becomes the stable state, as shown in Table 3. The energy gap disappearing in the DOS is due to the variation of Cr and Co atoms, as shown in Figure 3d.

Next, we investigate the valence configurations. Using the nominal valence states, the ordered double perovskite points to the state of $\text{Bi}_2^{3+}(\text{BB}')^{6+}\text{O}_6^{2-}$. According to the magnitude and spin direction of the Cr/Co magnetic moment, the transition metal atoms *B* and *B'* of $\text{Bi}_2\text{CrCoO}_6$ can have valence configurations of $\text{Cr}^{+3}(3d^3)$ and $\text{Co}^{+3}(3d^6)$, so that $\text{Cr}^{3+}(3d^3 4s^0: t^3_{2g} e^0_g)$ at $S = 3/2$ and $\text{Co}^{3+}(3d^6 4s^0: t^6_{2g} e^0_g)$ at $S = 0$. Moreover, in the actual materials, the electronic number from the mentioned ionic model, with simplified valence configurations, would be redistributed in consideration of the process of hybridization among Cr (Co) *3d* and O *2p* orbitals. This results in Cr and Co having total electron numbers of 4.4 and 7.3 for the *d* orbitals, implying the valence states of $\text{Cr}^{+1.6}(3d^{4.4})$, $\text{Co}^{+1.7}(3d^{7.3})$ for $\text{Bi}_2\text{CrCoO}_6$. For GGA + *U*, the valence states of $\text{Cr}^{+1.6}(3d^{4.4})$ and $\text{Co}^{+1.8}(3d^{7.2})$ are almost the same. Notably, the gap disappears for the GGA + *U* scheme.

For $\text{Bi}_2\text{CrNiO}_6$, the solid evidence of being half-metallic arises from the integer total magnetic moment of $4.0 \mu_B$ and spin-down energy gap of 0.65 (1.73) eV for both GGA and GGA+*U* processes. The process of GGA+*U* does not destroy the energy gap because the e_g and t_{2g} of Ni drop to a lower energy level, while the spin up channel maintains the conduction band. As a result, a stable FM-HM $\text{Bi}_2\text{CrNiO}_6$ is determined. The electron configuration for the ideal ionic model is $\text{Cr}^{+3}(3d^3 4s^0: t^3_{2g} e^0_g)$ at $S = 3/2$ and $\text{Ni}^{+3}(3d^7 4s^0: t^6_{2g} e^1_g)$ at $S = 1/2$. According to the data listed in Table 2, the calculated electron numbers of *d* orbitals for Cr and Ni are 4.4 and 8.3, giving the valence states of $\text{Cr}^{+1.6}(3d^{4.4})$ and $\text{Ni}^{+1.7}(3d^{8.3})$. In consideration of the GGA + *U* scheme, similar to the case with GGA, Cr and Ni have *d* orbital electron numbers of 4.3 and 8.3 and valence states of $\text{Cr}^{+1.7}(3d^{4.3})$ and $\text{Ni}^{+1.7}(3d^{8.3})$.

Following that, we explore the compound $\text{Bi}_2\text{FeNiO}_6$, in which the evidence of half-metallic property exists from the integer total magnetic moment of $4.0(6.0) \mu_B$ and energy gaps of 0.15 (1.68) eV in both GGA and GGA + *U* processes. In the case of the GGA + *U* scheme, however, the stability of the FM state disappears and AF becomes the final stable state. The gap near the Fermi level also flips and enlarges. This ensues from the significant *d* orbital variations of the PDOS for Fe and Ni between the FM and AF states.

The orbital hybridization among Fe t_{2g} , O *2p*, and Ni t_{2g} occurs mainly in the two parts of energy distribution from -7.5 eV to -0.8 eV and -0.2 eV to 1.0 eV, as shown in Figure 5a. The localized spin-to-spin interaction double exchange that enhances the HM property originates from the interaction of $\text{Fe}_{t_{2g}}\text{-O}_{2p}\text{-Ni}_{t_{2g}}$. However, when the case with GGA + *U* scheme is taken into consideration, the fact that the energy gap near the Fermi level flips from spin-up to spin-down and the *d* orbital distributions of Fe and Ni change largely results in the instability of the FM state. For the ideal ionic model of this compound, the electron configuration is $\text{Fe}^{+3}(3d^5 4s^0: t^5_{2g} e^0_g)$ at $S = 1/2$ and $\text{Ni}^{+3}(3d^7 4s^0: t^6_{2g} e^1_g)$ at $S = 1/2$. Consequently, after the calculation for the electron distribution of *d* orbitals of $\text{Bi}_2\text{FeNiO}_6$, the electron numbers for the *d* orbitals of Fe and Ni are 6.2 and 8.3. This result provides the real valence states of $\text{Fe}^{+1.8}(3d^{6.2})$ and $\text{Ni}^{+1.7}(3d^{8.3})$. When considering the GGA + *U* scheme, the valence states are calculated as $\text{Fe}^{+2.0}(3d^{6.0})$ and $\text{Ni}^{+1.7}(3d^{8.3})$. Only the calculation of $\text{Bi}_2\text{FeNiO}_6$ under the GGA scheme provides a stable state of FM-HM. For $\text{Bi}_2\text{FeNiO}_6$ under the GGA + *U* scheme, it becomes unstable as FM due to the energy gap flip and the changes in the *d* orbitals of Fe and Ni. To recap, we found stable FM-HM cases in $\text{Bi}_2\text{CrCoO}_6$ (GGA), $\text{Bi}_2\text{CrNiO}_6$ (GGA and GGA + *U*), as well as $\text{Bi}_2\text{FeNiO}_6$ (GGA).

3.2. FiM-HM Compounds: $\text{Bi}_2\text{FeZnO}_6$, $\text{Bi}_2\text{CrZnO}_6$ and $\text{Bi}_2\text{CoZnO}_6$

To determine the final stable state for $\text{Bi}_2\text{FeZnO}_6$, $\text{Bi}_2\text{CrZnO}_6$, and $\text{Bi}_2\text{CoZnO}_6$, we execute the calculation of structural optimization, in which all FM (FiM) states converge to either FiM or FM states. Consequently, in the GGA scheme, the calculated total energy differences ($\Delta E = \text{FM} - \text{AF}$) are listed as -58 , -60 , and -51 meV/f.u. for $\text{Bi}_2\text{FeZnO}_6$, $\text{Bi}_2\text{CrZnO}_6$, and $\text{Bi}_2\text{CoZnO}_6$, respectively, while with the GGA + *U* scheme, ΔE are recorded as 1125 , -73 , 99 meV/f.u. Furthermore, in the GGA scheme, energy gaps near Fermi level occur at the spin-down channel for $\text{Bi}_2\text{CrZnO}_6$ and at the spin-up channel for

$\text{Bi}_2\text{FeZnO}_6$ and $\text{Bi}_2\text{CoZnO}_6$. The energy gaps, in GGA, are reported as 0.97, 1.30, 0.85 eV, while with the GGA + U scheme, the energy gaps are 1.52 and 1.57 eV for $\text{Bi}_2\text{FeZnO}_6$ and $\text{Bi}_2\text{CrZnO}_6$. There are two energy gaps very close to Fermi level in $\text{Bi}_2\text{CoZnO}_6$ for spin-up and spin-down when applying the GGA + U scheme. We observe integer magnetic moments of $2.0 \mu_B/\text{f.u.}$ for $\text{Bi}_2\text{CrZnO}_6$ in both GGA and GGA + U schemes. On the other hand, the magnetic moments changed from 2.0 to $4.0 \mu_B/\text{f.u.}$ and 1.0 to $5.0 \mu_B/\text{f.u.}$ for $\text{Bi}_2\text{FeZnO}_6$ and $\text{Bi}_2\text{CoZnO}_6$ after the GGA + U scheme was given consideration. All the data are listed in Tables 2 and 3.

According to the PDOS of $\text{Bi}_2\text{FeZnO}_6$, the hybridization of Fe t_{2g} and O $2p$ occur in the range of energy from -7.5 eV to -1.0 eV for the spin-up channel and -0.5 eV to 0.5 eV for the spin-down channel. One weak magnetic moment $-0.022 \mu_B$ for Zn is induced by the asymmetry of the Zn e_g at the Fermi level. Hybridization between the Zn $3d$ and O $2p$ orbitals from -7.5 eV to -2.0 eV and -0.8 eV to 0.5 eV in the spin down channel is regarded as the main reason for the FiM state, as shown in Figure 6. The total electron numbers of d orbitals for Fe and Zn are 6.2 and 9.9, respectively. This gives the valence states of $\text{Fe}^{+1.8}(3d^{6.2})$ and $\text{Zn}^{+2.1}(3d^{9.9})$. When considering the ideal ionic model, the electron configuration is $\text{Fe}^{4+}(3d^4 4s^0: t^4_{2g} e^0_g)$ at $S = 1$, $\text{Zn}^{2+}(3d^{10} 4s^0: t^6_{2g} e^4_g)$ at $S = 0$. The electron configurations change a little after GGA + U , with $\text{Fe}^{+1.9}(3d^{6.1})$ and $\text{Zn}^{+1.9}(3d^{10.1})$. Not only does the band gap switch from a spin-up to a spin-down after GGA + U , but the ΔE is also extremely high. The energy instability has removed $\text{Bi}_2\text{FeZnO}_6$ (GGA + U) from candidacy as a stable FiM-HM.

Figure 7 illustrates the density of states (DOS) and PDOS of $\text{Bi}_2\text{CrZnO}_6$ for both GGA and GGA + U ($\text{Cr} = 5$, $\text{Zn} = 7$) schemes. With the GGA scheme, the hybridization between the Cr $3d$ and O $2p$ orbitals occurs mainly in the energy regions -7.0 eV to -1.0 eV and -0.5 eV to 0.5 eV, as shown in Figure 7a. Principally near the Fermi level (E_F), a spin-splitting at the spin-down channel and integer magnetic moment of $2.0 \mu_B/\text{f.u.}$ is regarded as the main features of HM. This asymmetry of the Zn e_g at the Fermi level gives Zn a weak magnetic moment, induced as -0.013 (GGA) and -0.008 (GGA + U) $\mu_B/\text{f.u.}$ These factors result in the FiM state. Next, we investigate the distribution of the electron configuration, for which the ideal model of $\text{Bi}_2\text{CrZnO}_6$ is $\text{Cr}^{4+}(3d^2 4s^0: t^2_{2g} e^0_g)$ at $S = 1$, $\text{Zn}^{2+}(3d^{10}: t^6_{2g} e^4_g)$ at $S = 0$. According to the following calculations, the total electron numbers of d orbitals for Cr and Zn are 4.4 and 10.0, respectively. This gives the valence states of $\text{Cr}^{+1.6}(3d^{4.4})$ and $\text{Zn}^{+2.0}(3d^{10.0})$. Considering the electron configuration with GGA + U scheme, it is also similar to the configuration with GGA. After GGA + U , the spin-down band gap slightly widens due to a shift in the Cr t_{2g} orbital and ΔE remains negative, showing a stable FiM-HM state. Similar to $\text{Bi}_2\text{FeZnO}_6$, illustrated in Figure 6, $\text{Bi}_2\text{CrZnO}_6$ is regarded as a stable FiM-HM for both GGA and GGA+ U schemes.

Finally, in the compound $\text{Bi}_2\text{CoZnO}_6$, the hybridization between Co t_{2g} and O $2p$ occurs in the two energy regions -7.0 eV to -0.6 eV at the spin-up channel and -1.0 eV to 0.4 eV at the spin-down channel, as shown in Figure 8a. There is a weak magnetic moment of $-0.013 \mu_B$ for the Zn atom due to the asymmetric distribution of Zn e_g at the Fermi level. The energy gap of 0.85 eV exists at the spin-up channel with GGA, while with the GGA + U scheme, there are energy gaps of 0.65 eV for the spin-up channel and 0.75 eV for the spin-down channel, resulting in an insulating material and not a half-metal. Considering the electron configuration, the suitable ionic model for $\text{Bi}_2\text{CoZnO}_6$ is $\text{Co}^{4+}(3d^5 4s^0: t^5_{2g} e^0_g)$ at $S = 1/2$, $\text{Zn}^{2+}(3d^{10}: t^6_{2g} e^4_g)$ at $S = 0$. After calculations, the total electron numbers of d orbitals for Co and Zn are estimated to be 7.2 and 9.9. With GGA, this results in the final valence states of $\text{Co}^{+1.7}(3d^{7.3})$ and $\text{Zn}^{+2.1}(3d^{9.9})$. The electron configurations are regarded as $\text{Co}^{+2.0}(3d^{7.0})$ and $\text{Zn}^{+2.0}(3d^{10.0})$ if GGA+ U is considered. Consequently, $\text{Bi}_2\text{CoZnO}_6$ (GGA) is determined to be a stable FiM-HM material.

3.3. AF Compounds: $\text{Bi}_2\text{CrCoO}_6$ and $\text{Bi}_2\text{FeNiO}_6$

In this section, we select two compounds, $\text{Bi}_2\text{CrCoO}_6$ and $\text{Bi}_2\text{FeNiO}_6$, as examples to discuss AF-based calculations because of their final stable states, with GGA + U schemes belonging to AF rather than FM. We illustrate the distribution of DOS and PDOS of $\text{Bi}_2\text{CrCoO}_6$ and $\text{Bi}_2\text{FeNiO}_6$ in Figures 9 and 10, respectively. Comparing the states of $\text{Bi}_2\text{CrCoO}_6$ in Figure 3 with Figure 9, the GGA+ U scheme

has changed the compound from a FM-HM to a stable AF-Insulator (AF-IS). Meanwhile, the GGA + U scheme changed $\text{Bi}_2\text{FeNiO}_6$ from a FM-HM to a stable AF-Metal as shown in Figures 5 and 10. When considering the AF-based states, the total magnetic moment is zero because the magnetic alignments of B and B' are anti-parallel, as shown in Table 2. Thus, this table only lists the magnetic moment for one site of B and B' and omits another site. In addition, for analysis of stability, the energy level of AF-IS $\text{Bi}_2\text{CrCoO}_6$ (GGA + U) is -61.827 eV/f.u. and AF-metal $\text{Bi}_2\text{FeNiO}_6$ (GGA + U) is -57.083 eV/f.u., shown in Table 3.

In view of the total electron numbers for the d orbitals in AF $\text{Bi}_2\text{CrCoO}_6$, Cr and Co have electron numbers of 4.4 and 7.3, implying the valence states of $\text{Cr}^{+1.6}(3d^{4.4})$, $\text{Co}^{+1.7}(3d^{7.3})$ for GGA. For GGA + U , the valence states are $\text{Cr}^{+1.6}(3d^{4.4})$ and $\text{Co}^{+1.9}(3d^{7.1})$. The PDOS distribution of AF $\text{Bi}_2\text{CrCoO}_6$ is similar to that of FM $\text{Bi}_2\text{CrCoO}_6$. Considering the distribution of AF $\text{Bi}_2\text{FeNiO}_6$, these results provide the valence states of $\text{Fe}^{+1.9}(3d^{6.1})$ and $\text{Ni}^{+1.7}(3d^{8.3})$ for GGA and $\text{Fe}^{+2.0}(3d^{6.0})$ and $\text{Ni}^{+1.7}(3d^{8.3})$ for GGA + U . All the AF data are listed in Tables 2 and 3. Finally, the stable states under GGA + U are AF-IS $\text{Bi}_2\text{CrCoO}_6$ and AF-metal $\text{Bi}_2\text{FeNiO}_6$. However, these two compounds are not HM material.

3.4. Double Exchange Interaction

The evidence of double exchange (DE), favoring ferromagnetism, is investigated in this section. Double exchange is related to the indirect exchange process constructed by two magnetic ions (BB') with localized spin S_i and S_j via local exchange. Such an exchange minimizes the kinetic energy of hopping electrons due to the alignment of neighboring magnetic ions (BB'). Hence, it typically exists in compounds with mixed valence magnetic ions, especially in the transition metal (TM) ions. There are two factors included here for DE: one is the localized spin at each TM ion site and the other is Hund's first rule, which shows that the localized spin will couple with the spin of the mobile electron. Such an effect is interpreted as the related characteristic scalar product ($S_i \cdot S_j$). The derivation of DE Hamiltonian in detail can be referred to in a previous study [34].

Figure 11a,b demonstrates a clear double exchange interaction between the BB' , $\text{Bi}_2\text{CrCoO}_6$ and $\text{Bi}_2\text{FeNiO}_6$. In the GGA scheme, for $B = \text{Cr}$ and $B' = \text{Co}$, the spin-up electrons transfer from occupied Co d to empty Cr d in the t_{2g} (spin-up state) via O 2p, accompanying the FM-based material. Notably, for $\text{Bi}_2\text{CrCoO}_6$, there is distinct double exchange among the interaction of $\text{Cr}_{t_{2g}}\text{-O}_{2p}\text{-Co}_{t_{2g}}$, while for $\text{Bi}_2\text{FeNiO}_6$, the double exchange originates from the interaction of $\text{Fe}_{t_{2g}}\text{-O}_{2p}\text{-Ni}_{t_{2g}}$.

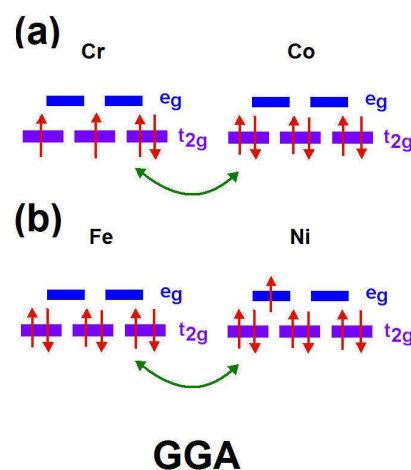


Figure 11. The double exchange interaction configuration for FM- $\text{Bi}_2\text{CrCoO}_6$ and FM- $\text{Bi}_2\text{FeNiO}_6$ in the GGA schemes. (a) Spin-up electron transfer between Co d and Cr d in the t_{2g} via O 2p (b) Spin-up electron transfer between Fe d and Ni d in the t_{2g} via O 2p.

Due to the fact that double exchange is a kind of mechanism happening between two magnetically active ions, i.e., partially-filled d -shells with different charge statuses, double exchange is irrelevant

here in compounds with Zn fully-filled d-orbitals. Consequently, it is not possible for the electrons from Co to hop to the Zn site (see the PDOS of Zn in Figure 7) so no double exchange exists here. Accordingly, the DE effect is not discussed for the cases of $\text{Bi}_2\text{FeZnO}_6$, $\text{Bi}_2\text{CrZnO}_6$, and $\text{Bi}_2\text{CoZnO}_6$. According to the electronic configurations mentioned in the discussion, we found evidence of double exchange existing in $\text{Bi}_2\text{CrCoO}_6$ and $\text{Bi}_2\text{FeNiO}_6$ FM-HM materials. The double exchange interaction of $B(t_{2g})\text{-O}(2p)\text{-}B'(t_{2g})$ configuration enhances the HM properties for these compounds and provides reasonable explanations for the stable magnetic states, magnetic moments, and energy gaps occurring in the spin channels.

4. Conclusions

This work has systematically investigated the electronic structure and magnetic properties of the double perovskite oxides $\text{Bi}_2\text{BB}'\text{O}_6$ (B, B' as $3d$ transitional metal). Accompanied by density functional theory (DFT) and full-structure optimization by generalized gradient approximation (GGA) and the strong correlation effect (GGA + U), a thorough examination of the possibility of HM materials under the four types of initial magnetic states was completed, i.e., ferromagnetic (FM), ferrimagnetic (FiM), antiferromagnetic (AF), and nonmagnetic (NM). The results indicate that there are six possible stable FM/FiM-HM materials, containing three FM-HM materials— $\text{Bi}_2\text{CrCoO}_6$, $\text{Bi}_2\text{CrNiO}_6$, and $\text{Bi}_2\text{FeNiO}_6$ —and three FiM-HM materials— $\text{Bi}_2\text{FeZnO}_6$, $\text{Bi}_2\text{CrZnO}_6$ and $\text{Bi}_2\text{CoZnO}_6$. When the Coulomb interaction correction (GGA + U) is considered, there are two promising candidates for half-metallic (HM) materials, which are $\text{Bi}_2\text{CrNiO}_6$ and $\text{Bi}_2\text{CrZnO}_6$. The evidence of double exchange interaction is disclosed from the $\text{Bi}_2\text{CrCoO}_6$ and $\text{Bi}_2\text{FeNiO}_6$ by the hybridization of magnetic ions' $3d$ orbitals via O $2p$. Moreover, we also explain why some calculated stable AF states are not also suitable candidates for HM material. Hopefully, through this research process using inorganic double perovskite oxides, we are able to provide a solid pathway for surveys of possible HM candidates and encourage scientists to execute further experimental research studies on these related HM materials.

Author Contributions: Conceptualization, H.-Z.L., C.-Y.H. and Y.-K.W.; Methodology, P.-H.L. and Y.-K.W.; Software, P.-H.L. and Y.-K.W.; Validation, P.-H.L., W.-F.W., Y.-F.C. and Y.-K.W.; Formal Analysis, H.-Z.L., C.-Y.H. and P.-H.L.; Investigation, H.-Z.L., C.-Y.H., P.-H.L. and Y.-K.W.; Resources, Y.-K.W.; Data Curation, P.-H.L.; Writing—Original Draft Preparation, H.-Z.L., C.-Y.H.; Writing—Review & Editing, P.-H.L., A.Z.-Z.Y. and Y.-K.W.; Visualization, P.-H.L., A.Z.-Z.Y. and Y.-K.W.; Supervision, W.-F.W., Y.-F.C. and Y.-K.W.; Project Administration, P.-H.L., and Y.-K.W.; Funding Acquisition, Y.-K.W.

Funding: This research received no external funding.

Acknowledgments: Y.-K.W. acknowledges the support by Taiwan Ministry of Science and Technology (MOST) through Grant No. MOST 107-2218-E-007-050. The calculations were conducted at the National Center for High-Performance Computing (NCHC) of Taiwan. The authors gratefully acknowledge the resource support from NCHC and the Computational Materials Research Focus Group. P.-H.L. also acknowledges the useful discussion with professor Swe-Kai Chen.

Conflicts of Interest: The authors declare no conflict of interest.

References

1. Park, J.H.; Vescovo, E.; Kim, H.J.; Kwon, C.; Ramesh, R.; Venkatesan, T. Direct evidence for a half-metallic ferromagnet. *Nature* **1998**, *392*, 794–796. [[CrossRef](#)]
2. Pickett, W.E.; Moodera, J.S. Half metallic magnets. *Phys. Today* **2001**, *54*, 39–44. [[CrossRef](#)]
3. Kobayashi, K.I.; Kimura, T.; Sawada, H.; Terakura, K.; Tokura, Y. Room-temperature magnetoresistance in an oxide material with an ordered double-perovskite structure. *Nature* **1998**, *395*, 677–680. [[CrossRef](#)]
4. Schwarz, K.J. CrO_2 predicted as a half-metallic ferromagnet. *Phys. F Met. Phys.* **1986**, *16*, 211–216. [[CrossRef](#)]
5. Jeng, H.T.; Guo, G.Y. First-principles investigations of orbital magnetic moments and electronic structures of the double perovskites $\text{Sr}_2\text{FeMoO}_6$, $\text{Sr}_2\text{FeReO}_6$, and Sr_2CrWO_6 . *Phys. Rev. B* **2003**, *67*, 094438. [[CrossRef](#)]
6. Chan, T.S.; Liu, R.S.; Guo, G.Y.; Hu, S.F.; Lin, J.G.; Chen, J.M.; Chang, C.R. Effects of B' -site transition metal on the properties of double perovskites Sr_2FeMO_6 ($M = \text{Mo}, \text{W}$): B' 4d–5d system. *Solid State Commun.* **2005**, *133*, 265–270. [[CrossRef](#)]

7. Wu, H. Electronic structure study of double perovskites A_2FeReO_6 ($A = Ba, Sr, Ca$) and Sr_2MMoO_6 ($M = Cr, Mn, Fe, Co$) by LSDA and LSDA + U. *Phys. Rev. B* **2001**, *64*, 125126. [[CrossRef](#)]
8. Meetei, O.N.; Erten, O.; Mukherjee, A.; Randeria, M.; Trivedi, N.; Woodward, P. Theory of half-metallic double perovskites. I. Double exchange mechanism. *Phys. Rev. B* **2013**, *87*, 165104. [[CrossRef](#)]
9. Erten, O.; Meetei, O.N.; Mukherjee, A.; Randeria, M.; Trivedi, N.; Woodward, P. Theory of half-metallic double perovskites. II. Effective spin Hamiltonian and disorder effects. *Phys. Rev. B* **2013**, *87*, 165105. [[CrossRef](#)]
10. Wang, Y.K.; Lee, P.H.; Guo, G.Y. Half-metallic antiferromagnetic nature of La_2VTcO_6 and La_2VCuO_6 from ab initio calculations. *Phys. Rev. B* **2009**, *80*, 224418. [[CrossRef](#)]
11. Coey, J.M.D.; Viret, M.; von Molnar, S. Mixed-valence manganites. *Adv. Phys.* **1999**, *48*, 167–293. [[CrossRef](#)]
12. Kronik, L.; Jain, M.; Chelikowsky, J.R. Electronic structure and spin polarization of $Mn_xGa_{1-x}N$. *Phys. Rev. B* **2002**, *66*, 041203. [[CrossRef](#)]
13. Park, M.S.; Kwon, S.K.; Toun, S.J.; Min, B.I. Half-metallic electronic structures of giant magnetoresistive spinels: $Fe_{1-x}Cu_xCr_2S_4$ ($x = 0.0, 0.5, 1.0$). *Phys. Rev. B* **1999**, *59*, 10018. [[CrossRef](#)]
14. Shirai, M.; Ogawa, T.; Kitagawa, I.; Suzuki, N. Band structures of zinc-blende-type $MnAs$ and $(MnAs)_1(GaAs)_1$ superlattice. *J. Magn. Magn. Mater.* **1998**, *177*, 1383–1384. [[CrossRef](#)]
15. Park, J.H.; Kwon, S.K.; Min, B.I. Electronic structures of III–V based ferromagnetic semiconductors: Half-metallic phase. *Phys. B* **2000**, *281*, 703–704. [[CrossRef](#)]
16. Chen, G.; Balents, L. Spin-orbit coupling in d^2 ordered double perovskites. *Phys. Rev. B* **2011**, *84*, 094420. [[CrossRef](#)]
17. Fuh, H.R.; Weng, K.C.; Liu, Y.P.; Wang, Y.K. Theoretical prediction of a new type of half-metallic materials in double perovskite $Pb_2BB'O_6$ ($B, B' = 3d$ transition metal) via First-Principle calculations. In *Spin*; World Scientific Publishing Company: Singapore, 2014; Volume 4, p. 1450001.
18. Li, Z.; Cho, Y.; Li, X.; Li, X.; Aimi, A.; Inaguma, Y.; Alonso, J.A.; Fernandez-Diaz, M.T.; Yan, J.; Downer, M.C.; et al. New mechanism for ferroelectricity in the perovskite $Ca_{2-x}Mn_xTi_2O_6$ synthesized by spark plasma sintering. *J. Am. Chem. Soc.* **2018**, *140*, 2214–2220. [[CrossRef](#)]
19. Kojima, A.; Teshima, K.; Shirai, Y.; Miyasaka, T. Organometal Halide Perovskites as Visible-Light Sensitizers for Photovoltaic Cells. *J. Am. Chem. Soc.* **2009**, *131*, 6050–6051. [[CrossRef](#)]
20. Seo, J.; Noh, J.H.; Seok, S.I. Rational strategies for efficient perovskite solar cells. *Acc. Chem. Res.* **2016**, *49*, 562–572. [[CrossRef](#)]
21. Zuo, C.; Bolink, H.J.; Han, H.; Huang, J.; Cahen, D.; Ding, L. Advances in perovskite solar cells. *Adv. Sci.* **2016**, *3*, 1500324. [[CrossRef](#)]
22. Yang, W.S.; Park, B.-W.; Jung, E.H.; Jeon, N.J.; Kim, Y.C.; Lee, D.U.; Shin, S.S.; Seo, J.; Kim, E.K.; Noh, J.H.; et al. Iodide management in formamidinium-lead-halide-based perovskite layers for efficient solar cells. *Science* **2017**, *356*, 1376–1379. [[CrossRef](#)] [[PubMed](#)]
23. Unger, E.L. The PV-Researcher's Siren: Hybrid metal halide perovskites. *Curr. Opin. Green Sustain. Chem.* **2017**, *4*, 72–76. [[CrossRef](#)]
24. Zhou, X.; Jankowska, J.; Dong, H.; Prezhdo Oleg, V. Recent theoretical progress in the development of perovskite photovoltaic materials. *J. Energy Chem.* **2018**, *27*, 637–649. [[CrossRef](#)]
25. Li, Z.; Yin, W. Recent progress in Pb-free stable inorganic double halide perovskites. *J. Semicond.* **2018**, *39*, 071003. [[CrossRef](#)]
26. Kato, H.; Okuda, T.; Okimoto, Y.; Tomioka, Y. Structural and electronic properties of the ordered double perovskites A_2MReO_6 ($A = Sr, Ca$; $M = Mg, Sc, Cr, Mn, Fe, Co, Ni, Zn$). *Phys. Rev. B* **2004**, *69*, 184412. [[CrossRef](#)]
27. Tang, C.Q.; Zhang, Y.; Dai, J. Electronic and magnetic structure studies of double perovskite Sr_2CrReO_6 by first-principles calculations. *Solid State Commun.* **2005**, *133*, 219–222. [[CrossRef](#)]
28. Philipp, J.B.; Majewski, P.; Alff, L.; Erb, A.; Gross, R.; Graf, T.; Brandt, M.S.; Simon, J.; Walther, T.; Mader, W.; et al. Structural and doping effects in the half-metallic double perovskite A_2CrWO_6 ($A = Sr, Ba, and Ca$). *Phys. Rev. B* **2003**, *68*, 144431. [[CrossRef](#)]
29. Liu, Y.P.; Fuh, H.R.; Xiao, Z.R.; Wang, Y.K. Theoretical prediction of half-metallic materials in double perovskites $Sr_2Cr(Co)B'O_6$ ($B' = Y, La, Zr, and Hf$) and $Sr_2V(Fe)B'O_6$ ($B' = Zr$ and Hf). *J. Alloys Compd.* **2014**, *586*, 289–294. [[CrossRef](#)]

30. Nakamura, T.; Choy, J.H. Determination of ionic valency pairs via lattice constants in ordered perovskites (ALa)(Mn²⁺Mo⁵⁺)O₆ (A = Ba, Sr, Ca) with applications to (ALa)(Fe³⁺Mo⁴⁺)O₆, Ba₂(Bi³⁺Bi⁵⁺)O₆ and Ba₂(Bi³⁺Sb⁵⁺)O₆. *J. Solid State Chem.* **1977**, *20*, 233–244. [[CrossRef](#)]
31. Zener, C. Interaction between the d-Shells in the Transition Metals. II. Ferromagnetic Compounds of Manganese with Perovskite Structure. *Phys. Rev.* **1951**, *82*, 403. [[CrossRef](#)]
32. Anderson, P.W.; Hasegawa, H. Considerations on double exchange. *Phys. Rev.* **1955**, *100*, 675. [[CrossRef](#)]
33. Pradhan, K.; Jena, P. Double exchange mediated ferromagnetic coupling between Co atoms in dicobalt complex. *Appl. Phys. Lett.* **2011**, *99*, 153105. [[CrossRef](#)]
34. Nolting, W.; Ramakanth, A. *Quantum Theory of Magnetism*; Springer: Heidelberg, Germany; Dordrecht, The Netherlands; London, UK; New York, NY, USA, 2009; ISBN 978-3-540-85415-9. [[CrossRef](#)]
35. Solovyev, I.V.; Terakura, K. Zone Boundary Softening of the Spin-Wave Dispersion in Doped Ferromagnetic Manganites. *Phys. Rev. Lett.* **1999**, *82*, 2959. [[CrossRef](#)]
36. Solovyev, I.V.; Terakura, K. *Electronic Structure and Magnetism of Complex Materials*; Singh, D.J., Papaconstantopoulos, D.A., Eds.; Springer: Berlin, Germany, 2003.
37. Kohn, W.; Sham, L.J. Self-Consistent Equations Including Exchange and Correlation Effects. *Phys. Rev.* **1965**, *140*, A1133. [[CrossRef](#)]
38. Perdew, J.P.; Burke, K.; Ernzerhof, M. Generalized gradient approximation made simple. *Phys. Rev. Lett.* **1996**, *77*, 3865. [[CrossRef](#)] [[PubMed](#)]
39. Kresse, G.; Hafner, J. Ab initio molecular dynamics for open-shell transition metals. *Phys. Rev. B* **1993**, *48*, 13115. [[CrossRef](#)]
40. Kresse, G.; Furthmüller, J. Efficiency of ab-initio total energy calculations for metals and semiconductors using a plane-wave basis set. *Comput. Mater. Sci.* **1996**, *6*, 15–50. [[CrossRef](#)]
41. Kresse, G.; Furthmüller, J. Efficient iterative schemes for ab initio total-energy calculations using a plane-wave basis set. *Phys. Rev. B* **1996**, *54*, 11169. [[CrossRef](#)]
42. Solovyev, I.V.; Dederichs, P.H.; Anisimov, V.I. Corrected atomic limit in the local-density approximation and the electronic structure of d impurities in Rb. *Phys. Rev. B* **1994**, *50*, 16861–16871. [[CrossRef](#)]



© 2019 by the authors. Licensee MDPI, Basel, Switzerland. This article is an open access article distributed under the terms and conditions of the Creative Commons Attribution (CC BY) license (<http://creativecommons.org/licenses/by/4.0/>).